Renewable Energy, Environment, and Power Quality Journal (REE&PQJ)
ISSN:3020-531X
Volume 24, January 2026

Experimental test bench for validating grid-forming strategies in V2G applications

A. Ordono[1], J. Rodriguez-Gongora[1], F.J. Asensio[1], J.A Cortajarena[2], A. Sanchez-Ruiz[3], M. Zubiaga[2]

[1] Department of Electrical Engineering
Engineering School of Gipuzkoa, University of the Basque Country (UPV/EHU)
Avda. Otaola, 29, 20600 Eibar (Spain)
Phone/Fax number: +34 943 033036

[2] Department of Electronic Technology
Engineering School of Gipuzkoa, University of the Basque Country (UPVEHU)
Avda. Otaola, 29, 20600 Eibar (Spain)

[3] Department of Electronic Technology
Engineering School of Vitoria-Gasteiz, University of the Basque Country (UPV/EHU)
Nieves Cano 12, 01006 Vitoria-Gasteiz (Spain)

Abstract. An experimental platform is developed with the aim of evaluating the performance of grid forming strategies in bidirectional electric vehicle (EV) chargers. The test bench is developed connecting a battery simulator to a grid simulator using a power converter that acts as an EV charger. This EV charger is composed of two stages: a DC/DC that increases the DC voltage of the battery, and a DC/AC that exchanges active and reactive power with the grid. The interface between the EV charger and the grid is done using an LCL filter, which is designed to meet the power quality requirements of the grid standards. The controller is a cRIO-9040, which integrates the control algorithms for both DC/DC and DC/AC stages, and a high acquisition task (10 kHz). The results obtained in the test bench are compared with the simulations carried out in Matlab/Simulink, showing the appropriateness of the experimental setup to validate control algorithms.

Key words. Vehicle to grid (V2G), grid forming (GFM), test bench.

1. Introduction

With the increasing deployment of electric vehicles (EVs), Vehicle to Grid (V2G) applications have attracted the attention of researchers [1]. In V2G applications, the EV charger provides a bidirectional power flow between the battery and the grid. Hence, apart from charging the battery, it can be used to support the grid. Even if the power of a single EV charger is small compared to the grid, this approach could be extended to several aggregated chargers [2]. In this context, V2G chargers could work as a distributed energy storage device, replacing static battery applications and reducing investment costs [3].

V2G can provide several services to the grid [4]. Among the most interesting ones, those that require high power and low energy are the most profitable for EVs, as they will have minimal impact on battery degradation. Inertia emulation, fast frequency regulation and voltage support are usually suggested for V2G applications [5]. Moreover, these services can be integrated inside the V2G charger without the need of a communication link, using only local measurements.

When interfacing the grid, V2G chargers could operate using two different strategies: grid following (GFL) and grid forming (GFM) [6]. GFL, based on a current control and a Phase-Locked Loop, is the most common approach. However, it has shown stability issues as power converter penetration increase [7]. GFM, on the other hand, can contribute to the stability of the grid by behaving as a voltage source behaviour and mimicking synchronous generators. However, GFM strategies are not still mature and further research is required [8].

This work will describe an experimental test bench developed to evaluate the performance of GFM strategies in V2G chargers. This work will focus on the AC stage of the power converter, as the DC/DC stage was already covered in a previous work [9]. The proposed test bench provides high flexibility to develop and test different algorithms on V2G scenarios and could be used to evaluate the performance of the system under different parameters.

The structure of the work is as follows. Section 2 provides a description of the topology of the system. Section 3 will describe design of the LCL filter that is used to ensure the power quality of the system. Section 4 will describe the bas GFM algorithm that has been developed for the current application. Section 5 will focus on the validation of the

test bench, comparing the experimental and simulation data. Finally, conclusions are given in Section 6.

2. System description

The proposed test bench scheme is shown in Figure 1. It is composed of a DC voltage source, followed by a DC/DC and a DC/AC stage, connected through an intermediate DC bus. The specifications for the DC/AC stage, which is the focus of this work, are given in Table 1. The rated power and the rated line voltage will be used as base values to provide all the data in per unit (pu) system along the work.

Table 1. Rated values of the DC/AC stage.

Parameter	Rated value
Power (P_n)	625 W
Line Voltage (V_{gn})	200 Vrms
Grid frequency (f_n)	50 Hz
Switching Frequency (f_{sw})	10 kHz
DC bus voltage (V_{bus})	300 Vdc

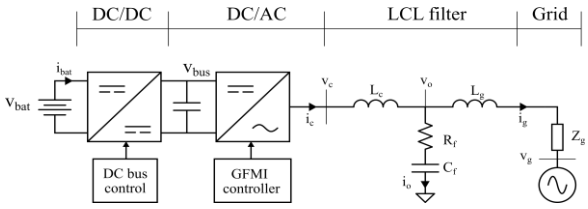

Figure 1. Schematic of the electrical test bench.

The DC/AC stage is connected to the grid using a LCL filter to meet the power quality requirements. It is composed by an inverter-side inductor L_c, a grid-side inductor L_g and a filter capacitor C_f. A damping resistor R_f is added in series to the capacitor to damp the resonance peak of the filter.

3. LCL filter design

The LCL filter components are designed attending to converter current ripple, voltage drop, reactive power and power quality requirements [10]:

A. L_c design

L_c is usually selected to be determined between a minimum ($L_{c,min}$) and maximum value ($L_{c,max}$). The minimum inductance is determined by the maximum allowable ripple under rated operating conditions. Its value in H is given by:

$$L_{c,min} = \frac{M_r V_{bus}}{2\lambda_{Lc} I_{c(1)} f_{sw}} \quad (1)$$

Where,
- M_r is the modulation index. A maximum value of 1.15 is expected under 3rd harmonic injection.
- λ_{Lc} is the current ripple coefficient. It is defined as the ratio between the peak-to-peak ripple and the root mean square (rms) value of the rated grid current.
- $I_{c(1)}$ denotes the rms value of the fundamental component of the rated grid current.

Lower current ripple will lead to lower semiconductor losses and higher efficiency. However, it will require a higher DC voltage level due to the voltage drop in the inductor. $L_{c,max}$ is selected to limit the voltage drop in the inductor:

$$L_{c,max} = \frac{\lambda_{Lv} V_{go}}{\omega_n I_{c(1)}} \cong \frac{\lambda_{Lv} V_{gn}}{\omega_n I_{c(1)}} \quad (2)$$

Where,
- λ_{Lv} is the voltage drop coefficient. It is the ratio between the voltage drop and the capacitor voltage at rated conditions.
- V_o is the capacitor voltage rated rms value. Assuming a negligible voltage drop across the grid-side inductor, it can be approximated to the grid voltage (V_{gn}).
- ω_n is the nominal angular speed of the grid.

Table 2 summarizes the design criteria and results for L_c. The final value of the inductance has been selected according to the available off-the-shelf components.

Table 2. L_c design criteria and results.

Parameter	Value
Current ripple factor (λ_{Lc})	0.3 pu
Voltage factor (λ_{Lv})	0.05 pu
Minimum inductance ($L_{c,min}$)	0.044 pu (9 mH)
Maximum inductance ($L_{c,max}$)	0.05 pu (10 mH)
Selected inductance (L_c)	0.05 pu (10 mH)
Rated current (I_{cn})	1 pu (1.8 Arms)

B. C_f design

The filter capacitance is chosen according to reactive power limitations. The higher the capacitance, the larger the reactive power of the filter. This will increase the current handled by the semiconductors, increasing its losses. C_f is selected considering restrained reactive power injection. Its value in F is given by:

$$C_f = \lambda_C \cdot \frac{P_n}{3\omega_n V_{gn}^2} \quad (3)$$

Where,
- λ_C is the reactive power ratio. It is defined as the reactive power of the capacitor to the active power of the converter at rated conditions.

Table 3 summarizes the design criteria and results for C_f.

Table 3. C_f design criteria and results.

Parameter	Value
Reactive power ratio λ_c	0.05 pu
Filter capacitance C_f	0.05 pu (2.5 uF)
Capacitor current (I_{on})	0.05 pu (0.09 Arms)

C. L_g design

The design criteria of grid-side inductance is based on grid current power quality requirements. The filter attenuation must be large enough to reduce harmonics amplitude

below certain threshold determined by standards. The minimum L_g value (in H) to meet each harmonic attenuation is given by:

$$L_{g,min} = \frac{1}{L_c C_f \left(h\omega_{gn}\right)^2 - 1} \cdot \left(L_c + \frac{\left|V_c\left(jh\omega_{gn}\right)\right|}{h\omega_{gn}\lambda_h I_{g(1)}} \right) \quad (4)$$

Where,
- h is the harmonic order.
- $\left|V_c\left(jh\omega_{gn}\right)\right|$ is the converter voltage h-th harmonic rms value.
- λ_h is the maximum allowed ratio of the h-th grid current harmonic respect to the fundamental. For this application, the values given in IEEE Std. 1547-2003 are used [11].
- $\boldsymbol{I_{g(1)}}$ is the rms value of the fundamental component of the rated grid current.

The design of $\boldsymbol{L_g}$ is obtained in simulation obtaining a value of 0.006 pu (1.2 mH). The current harmonic content of the grid current at rated conditions is given in Figure 2, where these values are compared with the maximum allowed values of the standard. The total harmonic distortion is 1.76%. The results consider the damping resistor selected in the next subsection.

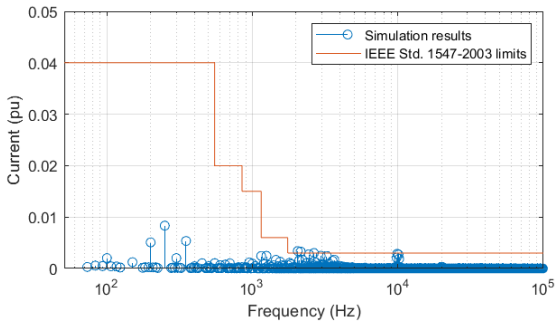

Figure 2. Grid current harmonic spectrum for selected L_g.

D. R_f design

A LCL filter will introduce a resonance peak that could limit the stability of the power converter. To damp the resonance, several strategies can be used, both active and passive. This work considers a passive strategy in which a resistor is connected in series with C_f. The transfer function of the damped LCL filter is given by:

$$G_{LCL}(s) = \frac{i_g(s)}{v_c(s)} = \frac{1 + RC_f s}{L_c L_g C_f s^3 + RC_f\left(L_c + L_g\right)s^2 + \left(L_c + L_g\right)s} \quad (5)$$

The bode response of the system with different damping resistances is given in Figure 3 A high damping resistor will provide a better damping of the resonance, but it will also reduce grid current attenuation at high frequencies. A proper trade-off is achieved for a damping resistor of 0.08 pu.

4. Controller description

The GFM control scheme for the V2G charger is presented in Figure 4. The schematic is presented in per unit notation, where ω_b is the base angular speed in rad/s ($\omega_b = \omega_r$). Table 4 summarizes the control parameters. The following subsections will describe the main control blocks.

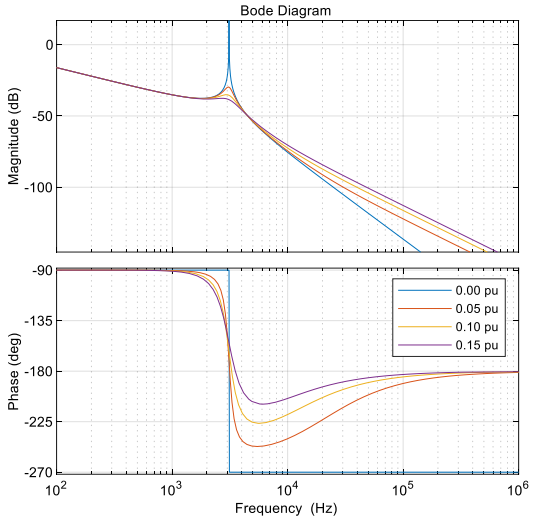

Figure 3. LCL filter response under different damping resistors.

Table 4. Grid forming controller parameters.

	Parameter	Rated value
Current Controller	k_p	0.49
	k_i	18.9
Virtual Admittance	R_v	0.06 pu
	L_v	0.3 pu
PSL	H	4 s
	D_p	50 pu
RPC	τ_q	20 ms
	m_q	0.1 pu

A. Power Synchronization Loop (PSL)

Opposite to GFL strategy, in which the angular frequency and position are obtained directly from the grid by means of a PLL, GFM synchronization is made using a Power Synchronization Loop (PSL). The synchronization is based on power balance, allowing them to operate in off-the-grid conditions. To provide dynamic frequency support to the grid, the proposed PSL generates the angular frequency and position based on a Virtual Synchronous Generator (VSG):

$$\frac{d\omega_r}{dt} = \frac{1}{2H}\left(P^* - P + D_P(\omega_r^* - \omega_r)\right) \quad (6)$$

Where,
- H is the virtual inertia coefficient in seconds.
- D_P is the damping coefficient in pu.
- P^* is the active power reference in pu.
- P is the measured active power in pu.
- ω_r is the PSL output angular frequency in pu.
- ω_r^* is the angular frequency reference in pu.

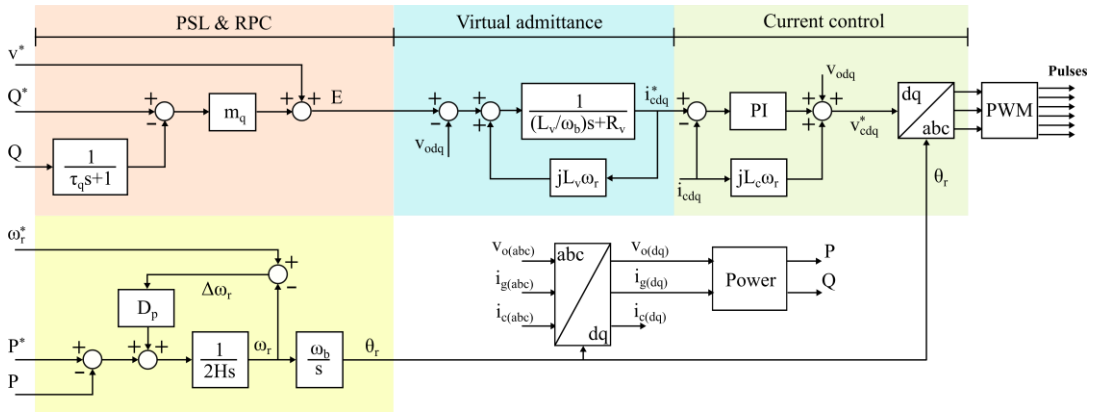

Figure 4. Grid forming controller of the DC/AC stage of the V2G charger.

B. Reactive Power Control (RPC)

The Reactive Power Control (RPC) generates the voltage reference (E) of the GFM, emulating the reactive power droop behaviour of SGs according to (7). A low-pass filter (LPF) is employed to remove high frequency ripple and adapt the reactive power loop dynamics.

$$E = v^* + m_q\left(Q^* - \frac{Q}{\tau_q s + 1}\right) \quad (7)$$

Where,
- v^* is the voltage command in pu.
- m_q is the reactive power droop coefficient in pu.
- Q^* is the reactive power command in pu.
- Q is the measured reactive power in pu.
- τ_q is the first order LPF time constant in seconds.

C. Virtual Admittance

The virtual admittance emulates an impedance between the converter and the grid. This control approach brings both simplification and stability improvement. On the one hand, it removes the need of a voltage controller. On the other hand, it can reduce the dynamics of the power controller and decouple active and reactive power regardless of the grid inductance to resistance ratio.

The virtual admittance dynamic equation in the dq frame is implemented using the following equation:

$$E - v_{odq} = R_v i^*_{cdq} + \frac{L_v}{\omega_b}\cdot\frac{di^*_{cdq}}{dt} + j\omega_r L_v i^*_{cdq} \quad (8)$$

Where,
- R_v and L_v denote the virtual resistance and inductance, respectively in pu.
- i^*_{cdq} is the converter current reference in dq frame in pu.
- v_{odq} is the capacitor voltage feedback in dq frame in pu.

A L_v = 0.3 pu and R_v = 0.06 pu is selected for the controller. These values are the typical internal impedances of synchronous generators.

D. Current Control

The inner current control loop is based on a classical PI controller. Decoupling terms and capacitor voltage feedforward are incorporated to improve the dynamics and decouple from the grid characteristics.

$$v^*_{cdq} = \left(k_p + \frac{k_i}{s}\right)\cdot\left(i^*_{cdq} - i_{cdq}\right) + j\omega_r L_c i_{cdq} + v_{odq} \quad (9)$$

Where,
- v^*_{cdq} is the converter voltage setpoint in pu.
- k_p is the proportional gain in pu.
- k_i is the integral gain in pu.

The controller is tuned using a modulus optimum approach, setting the bandwidth 20 times lower than the switching frequency, that is, 500 Hz [12].

5. Test bench description and validation

Figure 5 shows a schematic of the test bench. The EV battery is emulated using a Mean Well BIC-2200 bidirectional power supply, providing 96 Vdc. A Pacific Power 320-AMX emulates a 200 Vrms 3-phase power grid. Both the DC/DC and the DC/AC stages are based on Dutt INF-50 inverters. The passive elements (DC/DC choke and LCL filter) and the sensors are off-the-self components. Sensors and power inverters are connected to a National Instruments cRIO-9040, which will run the control algorithms on real-time. The controller is managed through an HMI, which will also receive the high-speed acquisition from the controller. An acquisition task running at 10 kHz in the FPGA of the cRIO will capture sensor data and internal control parameters, which are interesting for research purpose.

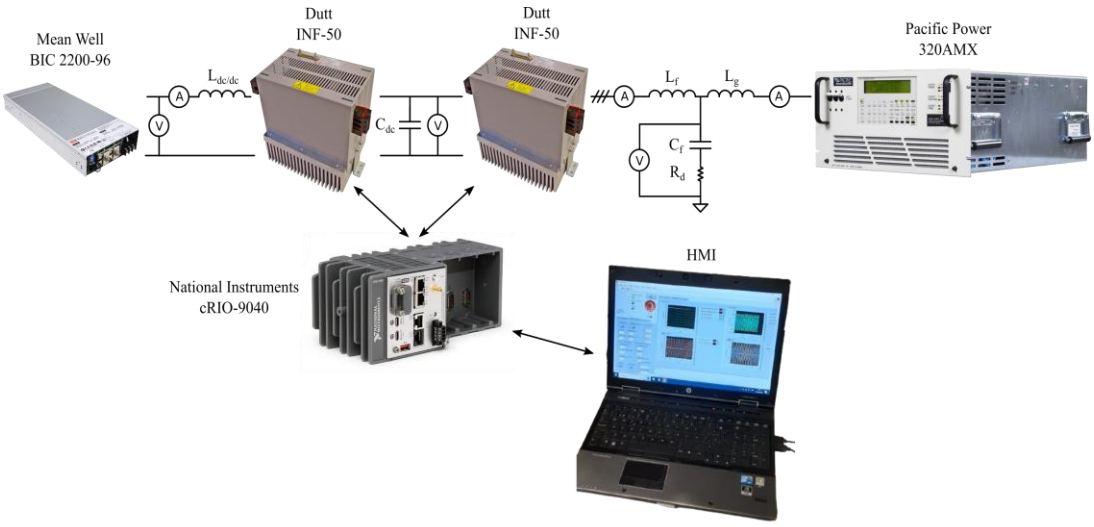

Figure 5. Schematic of the test bench for validating control strategies.

The following subsections will show some of the captures obtained in the test bench. These results are validated by comparing them with simulation results obtained in a Matlab/Simulink model. The model uses an average model for the power electronics, neglecting the switching frequency effect.

A. Power step setpoint

Figure 6 shows the V2G charger simulation and experimental results when an active power setpoint step of 0.1 pu is applied. The angular speed of the GFM control and the measured active and reactive power are shown.

The measured active power tracks the reference with the dynamics imposed by the PSL and the virtual admittance of the system. Both simulation and experimental power match each other, validating the operation of the test bench. During the active power transient, the angular speed of the GFM controller also shows a transient. This transient is related to the angle shift that is required between the GFM and the grid to exchange active power.

The active power setpoint will also produce a slight perturbation on the reactive power exchanged with the grid. The modification of the reactive power occurs because the active and reactive power decoupling in GFM is not perfect. The coupling of the power will be higher as the inductance to resistance ratio decreases. In this case, the inductance to resistance ratio of the system is determined by the virtual impedance ratio, which is five.

B. Grid frequency perturbation

Figure 7 shows the V2G charger simulation and experimental results for the case of a perturbation in the grid frequency. In this case, a perturbation of 0.002 pu occurs at t = 1 s. As in the previous case, angular speed and active and reactive power are shown.

When the frequency of the grid, the V2G charger will provide inertia and primary frequency support to the grid. The transient will be determined by H and D_p coefficients,

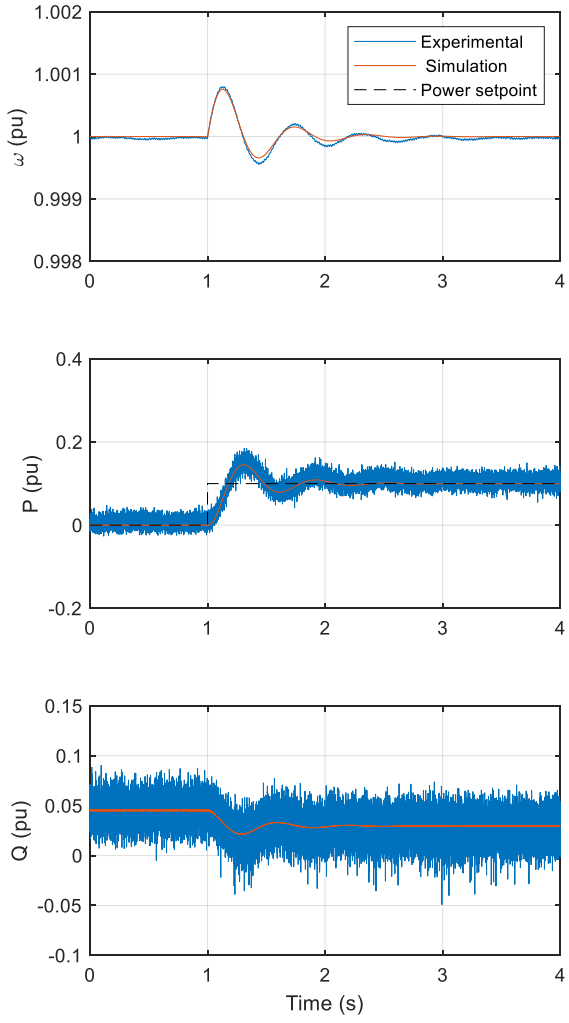

Figure 6. Simulation and experimental data under a power setpoint step of 0.1 pu

whereas the steady-state value will only depend on the latter. The steady-state active power exchange after the perturbation is -0.1 pu, which is the product of the damping of the controller (50 pu) and the frequency deviation (0.002 pu). The sign of the active power indicates that the active power is being absorbed by th

V2G charger, which is the expected response when the grid frequency increases. A grid frequency reduction will lead to an injection of active power.

As in the previous case, a slight perturbation on the reactive power exchange can be appreciated since active and reactive power are not 100% decoupled.

6. Conclusion

This paper has described the experimental test bench for evaluating the performance of grid forming algorithms in V2G applications. The work has focused on the AC side of the EV charger, focusing on the design of the LCL filter and the grid-forming algorithm that manages the DC/AC stage.

The proposed platform provides high versatility for developing different control strategies, and it could be used to evaluate the impact of different parameters on the performance of the system. Moreover, the test bench includes a real-time fast acquisition task that is interesting for research purposes, as it does not only capture sensor data, but also internal control signals.

The experimental results that have been obtained in the test bench match the simulation results, validating the design of the experimental setup.

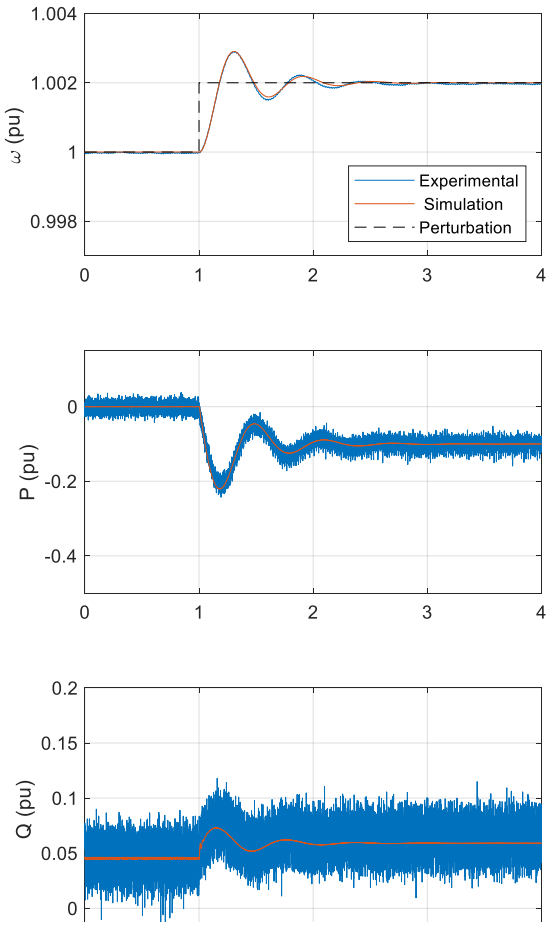

Figure 7. Simulation and experimental data under a frequency perturbation of 0.002 pu

Acknowledgement

The authors gratefully acknowledge the support from the Basque Government (ELKARTEK KK-2022/00100).

References

[1] M. İnci, M. M. Savrun, y Ö. Çelik, «Integrating electric vehicles as virtual power plants: A comprehensive review on vehicle-to-grid (V2G) concepts, interface topologies, marketing and future prospects», *Journal of Energy Storage*, vol. 55, p. 105579, nov. 2022, doi: 10.1016/j.est.2022.105579.

[2] Y. Jin, B. Yu, M. Seo, y S. Han, «Optimal Aggregation Design for Massive V2G Participation in Energy Market», *IEEE Access*, vol. 8, pp. 211794-211808, 2020, doi: 10.1109/ACCESS.2020.3039507.

[3] M. A. Hannan *et al.*, «Vehicle to grid connected technologies and charging strategies: Operation, control, issues and recommendations», *Journal of Cleaner Production*, vol. 339, p. 130587, mar. 2022, doi: 10.1016/j.jclepro.2022.130587.

[4] K. Sevdari, L. Calearo, P. B. Andersen, y M. Marinelli, «Ancillary services and electric vehicles: An overview from charging clusters and chargers technology perspectives», *Renewable and Sustainable Energy Reviews*, vol. 167, p. 112666, oct. 2022, doi: 10.1016/j.rser.2022.112666.

[5] A. Ordoño, F. J. Asensio, J. I. San Martín, M. González-Pérez, y Cortajarena, Jose Antonio, «Impact of electric vehicles fast frequency regulation and charging strategies on grid frequency stability», *RE&PQJ*, vol. 21, n.º 1, pp. 132-137, jul. 2023, doi: 10.24084/repqj21.247.

[6] Y. Li, Y. Gu, y T. C. Green, «Revisiting Grid-Forming and Grid-Following Inverters: A Duality Theory», *IEEE Trans. Power Syst.*, vol. 37, n.º 6, pp. 4541-4554, nov. 2022, doi: 10.1109/TPWRS.2022.3151851.

[7] X. Zhao y D. Flynn, «Stability enhancement strategies for a 100% grid-forming and grid-following converter-based Irish power system», *IET Renewable Power Generation*, vol. 16, n.º 1, pp. 125-138, 2022, doi: 10.1049/rpg2.12346.

[8] R. Musca, A. Vasile, y G. Zizzo, «Grid-forming converters. A critical review of pilot projects and demonstrators», *Renewable and Sustainable Energy Reviews*, vol. 165, p. 112551, sep. 2022, doi: 10.1016/j.rser.2022.112551.

[9] M. González-Pérez, F. J. Asensio, y J. I. San Martín, «Design of a bi-directional DC/DC converter for EV chargers oriented to V2G applications», *REPQJ*, vol. 20, pp. 198-203, sep. 2022, doi: 10.24084/repqj20.262.

[10] X. Ruan, X. Wang, D. Pan, D. Yang, W. Li, y C. Bao, *Control Techniques for LCL-Type Grid-Connected Inverters*. en CPSS Power Electronics Series. Singapore: Springer Singapore, 2018. doi: 10.1007/978-981-10-4277-5.

[11] «IEEE Standard for Interconnecting Distributed Resources with Electric Power Systems», *IEEE Std 1547-2003*, pp. 1-28, jul. 2003, doi: 10.1109/IEEESTD.2003.94285.

[12] A. Ordono, F. J. Asensio, J. A. Cortajarena, J. I. S. Martín, y M. González-Pérez, «Tuning of Dual-Loop Grid-Forming Inverters for Stable Operation Under Different Grid Conditions», en *IECON 2023- 49th Annual Conference of the IEEE Industrial Electronics Society*, Singapore, Singapore: IEEE, oct. 2023, pp. 1-6. doi: 10.1109/IECON51785.2023.10312182.